Theor Chem Acc (2012) 131:1182
DOI 10.1007/s00214-012-1182-2

REGULAR ARTICLE

Computational modelling of de novo synthesis of Dibenzofuran: oxidative pathways of Pyrene and Benzodibenzofuran

Ugo Cosentino · Demetrio Pitea · Giorgio Moro

Received: 20 July 2011 / Accepted: 9 November 2011 / Published online: 2 March 2012

Abstract The dominating route to polychlorinated Dibenzo-*p*-dioxin and Dibenzofuran formation in the "cold zones" of flue gas cleaning systems of municipal solid waste incinerators is the so-called de novo synthesis, that is, carbonaceous matrix burnoff with simultaneous oxidation and chlorination reactions. Pyrene (**1**) and Benzodibenzofuran (**2**) were chosen as the model compounds of carbonaceous material present in fly ash. Possible routes of Dibenzofuran formation by oxidative pathways of compounds (**1**) and (**2**) were investigated by theoretical calculations at the density functional theory level. The key intermediate peroxy radical, formed by reaction with molecular oxygen, can follow three main paths leading to Dibenzofuran. In the kinetically favourite path, the highest energetic barriers (25–30 kcal mol^{-1}) are encountered in the steps where CO molecules are released from ketene-like structures. These findings agree with previously reported temperature-programmed desorption results on CO desorption. Moreover, along this path, phenanthrene and biphenyl intermediates are formed, in agreement with the detection of these products in previously reported experimental Pyrene oxidation. Along the preferred path, different steric constraints in compounds (**1**) and (**2**) play a role in determining the relative stability of the intermediates, while they have less influence on the energetic barriers. As a consequence, compounds (**1**) and (**2**) should present similar kinetic behaviour as they present similar energetic barriers.

Keywords Oxidation mechanism · Benzodibenzofuran · Pyrene · Dibenzofuran · DFT calculations

1 Introduction

Incineration and thermal decomposition of waste material frequently lead to the production of trace quantities of the pollutants Polychlorinated Dibenzo-*p*-dioxins (PCDD) and Dibenzofurans (PCDF). In order to minimize the emission of these pollutants, it is important to develop appropriate combustion technologies based on a deep knowledge of the detailed mechanisms of their formation and destruction.

PCDD/F yield in thermal systems is a balance between destruction and formation pathways. Since the activation energies of the destruction reactions are higher than those of the formation reactions, the net rate of production has maxima at certain temperatures [1].

On the basis of numerous experimental studies, it is now widely accepted that PCDD/Fs are formed through two main pathways, one homogeneous and the other heterogeneous [2–4].

The homogeneous pathway involves the reaction, at temperatures between 400 and 800 °C, of structurally related precursors in the gas phase, the most important and direct precursors being monocyclic aromatic compounds

Dedicated to Professor Vincenzo Barone and published as part of the special collection of articles celebrating his 60th birthday.

Electronic supplementary material The online version of this article (doi:10.1007/s00214-012-1182-2) contains supplementary material, which is available to authorized users.

U. Cosentino (✉) · D. Pitea
Dipartimento di Scienze dell'Ambiente e del Territorio, University of Milano-Bicocca, Piazza della Scienza 1, 20126 Milan, Italy
e-mail: ugo.cosentino@unimib.it

G. Moro
Dipartimento di Biotecnologie e Bioscienze, University of Milano-Bicocca, Piazza della Scienza 2, 20126 Milan, Italy

such as chlorinated phenols and chlorobenzenes. Heterogeneous pathways act in the 200–400 °C range on solid fly-ash surfaces and involve two routes. The first, the so-called de novo synthesis, proceeds through carbonaceous matrix burnoff with simultaneous oxidation and chlorination; the second takes place by the coupling of precursors. Both routes are catalyst-assisted, mainly due to copper and iron compounds.

The dominating route in PCDD/F formation in the "cold zones" of flue gas cleaning systems of municipal solid waste (MSW) incinerators and secondary not-ferrous metal smelters and sinter plants is de novo synthesis [3, 5].

The carbon source for de novo synthesis is the solid carbon matrix of fly ash, which has imperfect or degenerate graphitic structures, called turbostratic carbon crystallite, linked by amorphous regions, that is, aliphatic and alicyclic bridges [3]. Although the carbon layers in turbostratic carbon crystallite are similar to those in graphite, the layers are stacked randomly and disorientedly with larger interlayer spacing and are thus more easily attacked by chemical reactions. The main chemical fate of a carbonaceous matrix is carbon gasification, PCDD/F de novo synthesis being only a trace reaction in the low-temperature regime.

Dibenzofuran (DF) and PCDF formation has been investigated in several experimental studies using a wide variety of polycyclic aromatic hydrocarbons (PAH), and these have lead to the hypotheses on the species and mechanisms involved in DF formation. Perylene has been proposed as the basic molecular structure able to explain the PCDF pattern in fluidized bed incinerators [6, 7], and analyses of PAH emissions, particularly of DF, from the high-temperature oxidation of anthracene have been carried out [8]. From the CuO catalysed oxidation of different PAHs [9], it was found that DF formation prevailed in oxidative pathways where phenanthrene is the reagent or an intermediate.

Also, the oxidative destruction of DF was experimentally investigated [10–12], leading to the proposal of two different DF oxidation mechanisms, one in high regime temperatures (>1,200 K) and the other in low.

Theoretical methods were used to investigate the mechanistic aspects of PCDD/F formation and destruction. Formation mechanisms from structurally related precursors were investigated at the ab initio level in both the gas-phase and heterogeneous catalytic–assisted reactions [2]. Furthermore, oxidative [13, 14] and pyrolytic [15] decomposition routes of DF were investigated.

For a theoretical investigation into the mechanisms of PCDD/F formation and destruction, advantage can be taken of available detailed knowledge, both experimental and theoretical, for oxidation mechanisms in the combustion process of aromatic and unsaturated hydrocarbons. In the initial steps, the combustion reaction of these systems involves the formation of a radical species with the loss of a hydrogen atom, through reaction with other radical species present in the environment (O, OH, O_2H, etc.) or with molecular oxygen. Following this, the newly formed radical species reacts with the molecular oxygen to form a peroxy radical R-$OO^{\cdot}$. This is the key intermediate that can evolve following different pathways. The potential energy surface of vinyl [16], phenyl [17] and Dibenzofuranyl radical [13, 14] oxidation pathways was carefully investigated at the ab initio level, addressing the overall similarities of these systems with respect to reactions with O_2 [14]. Thermochemical parameters of the species involved in the mechanisms were also calculated [18–20]. The oxidation of molecular PAHs and one-layer graphite by H, HO, NO, NO_2, and NO_3 species was investigated to model soot particle formation [21].

The general aim of our research was a theoretical investigation into the mechanism of PCDD/PCDF formation by de novo synthesis, in order to support experimental studies focused on preventing and/or minimizing PCDD/F formation.

In the present study, we chose Pyrene (**1**) and Benzodibenzofuran (**2,** BDF) as the model compounds of carbonaceous material present in fly-ash and involved in de novo synthesis (Scheme 1). Solid-state ^{13}C NMR experiments have shown [22] that char has structures of randomly connected graphene clusters, consisting of 12–25 aromatic carbon atoms, corresponding to 3–7 benzene rings. Mass spectra analysis of PAHs in flames has shown a significant presence of species consisting of a highly condensed system of 6-membered rings [23]. On the basis of these findings, compound (**1**), consisting of four condensed aromatic rings, can be considered a "small size" molecular model representative of carbonaceous material involved in de novo synthesis. Moreover, also compound (**2**) was considered due to the presence of partially oxidized compounds in the fly-ash carbon matrix.

Here, we present the results of our computational study on the reaction pathways of Pyrene (**1**) and Benzodibenzofuran (**2,** BDF) involved in the de novo synthesis of DF (Scheme 2). Indeed, any investigation into possible pathways involved in oxidative decomposition reactions of

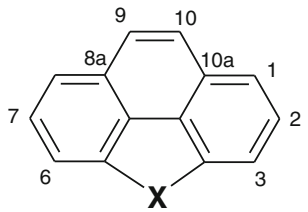

Scheme 1 Investigated systems and atomic numbering

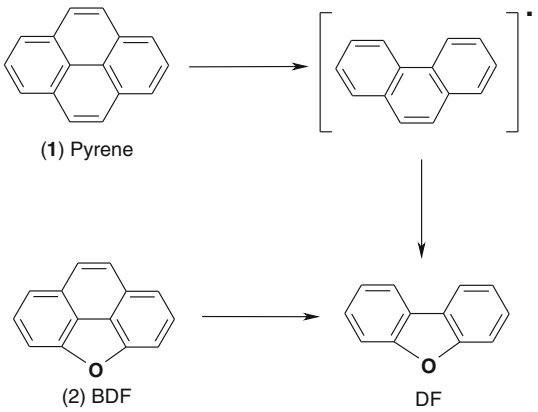

Scheme 2 Overall oxidative pathways for compounds (**1**) and (**2**)

aromatic hydrocarbons is a very demanding task, also for the simplest case, that is, the phenyl radical system [17]. In compounds (**1**) and (**2**) the presence of more than one ring significantly complicates the system, further increasing the number of possible reactive channels. Thus, given all the possible pathways, focusing only on those pathways involved in DF formation allows other competitive demolition pathways to be ignored and/or disregarded.

2 Computational details

All the calculations were performed with the Gaussian09 program [24]. Optimized geometries and harmonic vibrational frequencies of reactants, intermediates, products and transition states were calculated using the density functional theory (DFT) with the hybrid functional PBE1PBE [25] and the 6-311G** basis set. Spin-unrestricted calculations were performed for the radical systems. DFT densities and energies are known to be less affected by spin contamination than the corresponding unrestricted Hartree–Fock quantities [26]. In all the investigated radical systems, spin contamination was found to be negligible, the only exception being molecular systems made up by (Ar–O$^{\cdot}$) and the ground-state oxygen atom, O(^{3}P), deriving from the cleavage of the O–O bond in (Ar–OO$^{\cdot}$). Some caution is warranted in interpreting the results in these cases.

Intrinsic Reaction Coordinate (IRC) calculations were used to link reactants and products with their transition states. All the energy values reported include electron energies and Zero Point Energy (ZPE) corrections.

3 Test calculations on the phenyl peroxy system

The reliability of the PBE1PBE functional was tested by performing a preliminary investigation on the starting reaction channels of the phenyl peroxy radical, using the

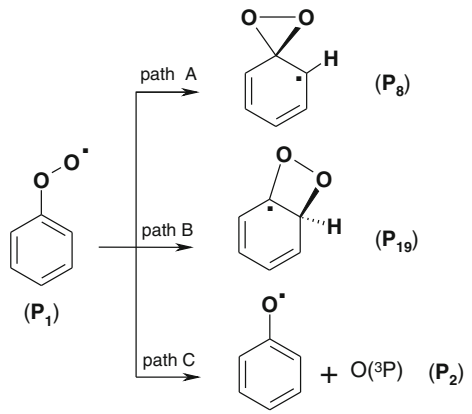

Scheme 3 Entry channel reactions of the phenyl peroxy radical. Molecular numbering as in Ref. [17]

Table 1 PBE1PBE/6-311++G** barriers (E_{att}, kcal mol^{-1}) and reaction energies ($E_{react} = E_{products} - E_{reagent}$, kcal mol^{-1}) for the starting reactions of (**P$_1$**) (Scheme 3). The B3LYP and G2 M(MP2) results from Ref. [17]

	PBE1PBE[a]		B3LYP[b]		G2 M(MP2)[b]	
	E_{att}	E_{react}	E_{att}	E_{react}	E_{att}	E_{react}
$P_1 \rightarrow P_8$	27.3	20.3	27.1	22.6	24.3	14.7
$P_1 \rightarrow P_{19}$	45.6	42.3	45.7	44.5	41.3	38.0
$P_1 \rightarrow P_2$	35.6	35.4	33.7	33.6	36.3	35.9

[a] PBE1PBE/6-311++G** geometries, present work

[b] B3LYP/6-311++G** geometries

6-311++G** basis set. According to a previous investigation [17], the starting reaction channels of the phenyl peroxy radical (**P$_1$**) can undergo three main reactions (Scheme 3). The (**P$_1$**) radical can isomerize to the (**P$_8$**) radical through the closure of a 3-membered ring (path A) or to the (**P$_{19}$**) through the closure of a 4-membered ring (path B). Path C involves the O–O cleavage and formation of the phenoxy radical and the ground-state oxygen atom, O(^{3}P).

Comparison of our results (Table 1) with those previously obtained [17] at the B3LYP and G2 M(MP2) levels [27] on B3LYP/6-311++G** geometries shows that the two functionals provide similar barriers and reaction energies as well as transition state geometries, with the PBE1PBE results in better agreement with the G2 M(MP2) results. Thus, the PBE1PBE functional is certainly suitable for modelling the reactivity of these systems.

4 Results

4.1 (Ar–OO$^{\cdot}$) formation

The initial step in the oxidative pathway of compounds (**1**) and (**2**) involves the formation of a radical species (Ar$^{\cdot}$)

Table 2 PBE1PBE/6-311G** relative energies (ΔE, kcal mol^{-1}) of the radical species of compounds (**1**) and (**2**), with respect to the parent compound

	ΔE (kcal mol^{-1})
(**1**$^{\cdot}$)$_{10}$	107.7
(**1**$^{\cdot}$)$_1$	108.1
(**1**$^{\cdot}$)$_2$	107.4
(**2**$^{\cdot}$)$_{10}$	107.4
(**2**$^{\cdot}$)$_1$	108.6
(**2**$^{\cdot}$)$_2$	107.0
(**2**$^{\cdot}$)$_3$	110.1

through the loss of a hydrogen atom by reaction with radical species (X$^{\cdot}$) present in the environment such as H, OH, O, alkyl groups or molecular oxygen. Depending on the environmental conditions, the barrier to overcome in this initial step will be quite different. To avoid the problem of having to choose a specific route to (**Ar**$^{\cdot}$) formation, we assumed the (**Ar**$^{\cdot}$) species to be already formed, regardless of the reactions involved.

The radicals obtained by the extraction of a hydrogen atom from compounds (**1**) and (**2**) present close relative energies (Table 2), and it can be expected that all of them will form, thus providing different reaction channels. However, as just the attack of molecular oxygen to C_{10} (or equivalent) position can lead to DF formation, only the (**1**$^{\cdot}$)**$_{10}$** and (**2**$^{\cdot}$)**$_{10}$** radicals are considered in the following (see Scheme 1 for numbering).

A barrier-less reaction between the radical species and the molecular oxygen leads to the (**Ar–OO**$^{\cdot}$) peroxy radicals. These peroxy radicals can follow different reaction pathways, involving intramolecular rearrangements of the peroxy radical or O–O bond scission, as in the case of the phenoxy radical [17]. However, of all these, only paths A–C, reported in Schemes 4, 5, 6, can lead to DF formation, and were considered for (**1-OO**$^{\cdot}$) and (**2-OO**$^{\cdot}$) evolution. Paths A and B involve intramolecular rearrangements of the peroxy radical, while path C involves O–O bond scission. All three paths (A–C) converge to a common intermediate (**A5**), and further evolution of (**A5**) finally leads to DF (Scheme 7).

Moreover, each of the considered paths can present several collateral paths, two converging to intermediates of the A–C paths, and thus investigated (Schemes 8, 9), the others evolving towards products other than DF and thus not considered.

4.2 (Ar–OO$^{\cdot}$) decomposition

Whenever possible, intermediates and transition states are named with the same label, without reference to the parent compound, (**1**) or (**2**). Relative energies with respect to (**Ar–OO**$^{\cdot}$) of the species involved along the different paths are reported in Tables 3 and 4 and Figs. 1, 2, 3.

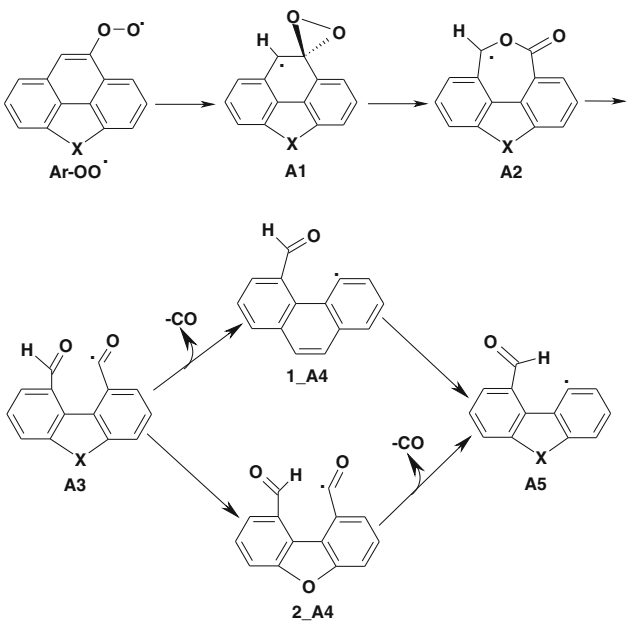

Scheme 4 Path A

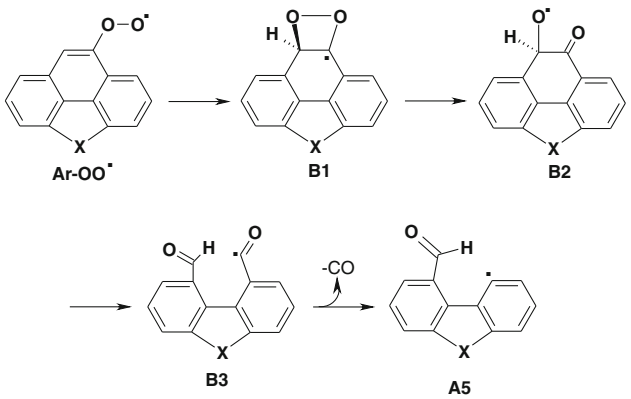

Scheme 5 Path B

Path A. The first step in this pathway (Scheme 4, Table 3, Fig. 1) consists in the isomerization of (**Ar–OO**$^{\cdot}$) to the dioxiranyl radicals (**A1**) through the closure of the 3-membered COO ring. The involved energetic barriers are reported in Table 3. In the next step, one of the oxygen atoms inserts into the C_9 and C_{10} bond to produce the 7-membered lactonic radical (**A2**), significantly more stable than (**A1**). Even though two isomers could be expected from the (**A1**) rearrangement (the oxygen atom could insert into the C_9–C_{10} or the C_{10}–C_{10a} bond), only the (**A2**) product is obtained, as confirmed by IRC calculations. Moreover, the stability of (**1_A2**) and (**2_A2**) differs notably. The difference can be explained on the basis of the different molecular geometries. Indeed, in (**2_A2**) the lactonic ring is planar, while in (**1_A2**) the phenanthrenic moiety constrains the carbonyl group outside the molecular

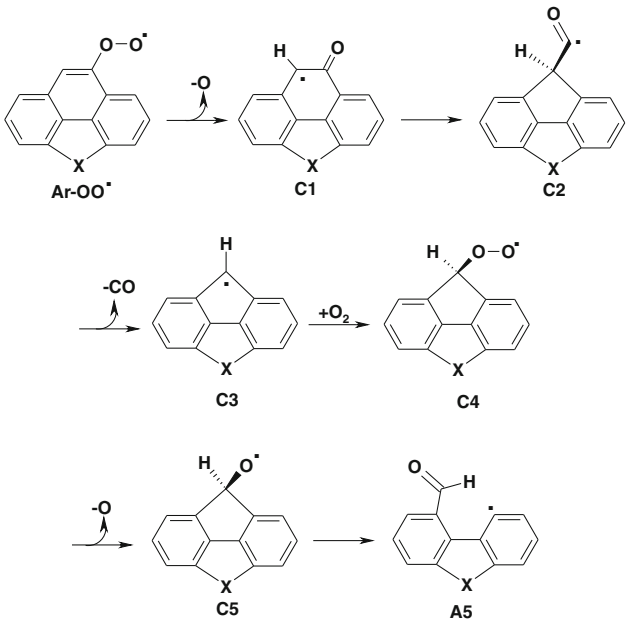

Scheme 6 Path C

plane. Along the (**A2**)–(**A5**) path, all intermediates and TSs from (**1**) present non-planar geometry due to the steric hindrance between the ortho substituents. On the contrary, derivatives from compound (**2**) are always planar; as a consequence, the path of compound (**2**) is at lower energies than that of compound (**1**).

Successively, the lactonic ring can be opened by stretching the O–C_{10} bond, providing the (**A3**) dicarbonyl intermediate. In the next two steps the paths of compounds (**1**) and (**2**) differ slightly. The (**1_A3**) intermediate evolves, losing one CO molecule and forming (**1_A4**) that undergoes a conformational rearrangement of the aldehydic group, providing (**1_A5**). In the case of (**2_A3**), the conformational rearrangement of the aldehydic group to (**2_A4**) is required before losing CO and yielding (**2_A5**). A van der Waals adduct between (**A5**) and the leaving CO molecule is observed in both cases.

A collateral path (Scheme 8, Table 4) starts from (**A2**) and converges to the (**C3**) intermediate along path C (see below). The lactonic radical (**A2**) fuses into the bicyclic intermediate (**$A2_1$**), a planar structure for compound (**1**) and a highly bent structure in (**2**), overcoming significant barriers due to the formation of a 4-membered ring. The (**C3**) intermediate is then obtained through the loss of one CO_2 molecule from (**$A2_2$**). Contrary to the (**A2**)–(**A5**) steps, here the path of compound (**2**) is at higher energy than that of compound (**1**), due to the constraints imposed by two condensed 5-membered rings.

Path B. The first step in this path (Scheme 5, Table 3, Fig. 2) involves an intramolecular cyclization in (**Ar–OO˙**) by the terminal oxygen atom of the peroxy group,

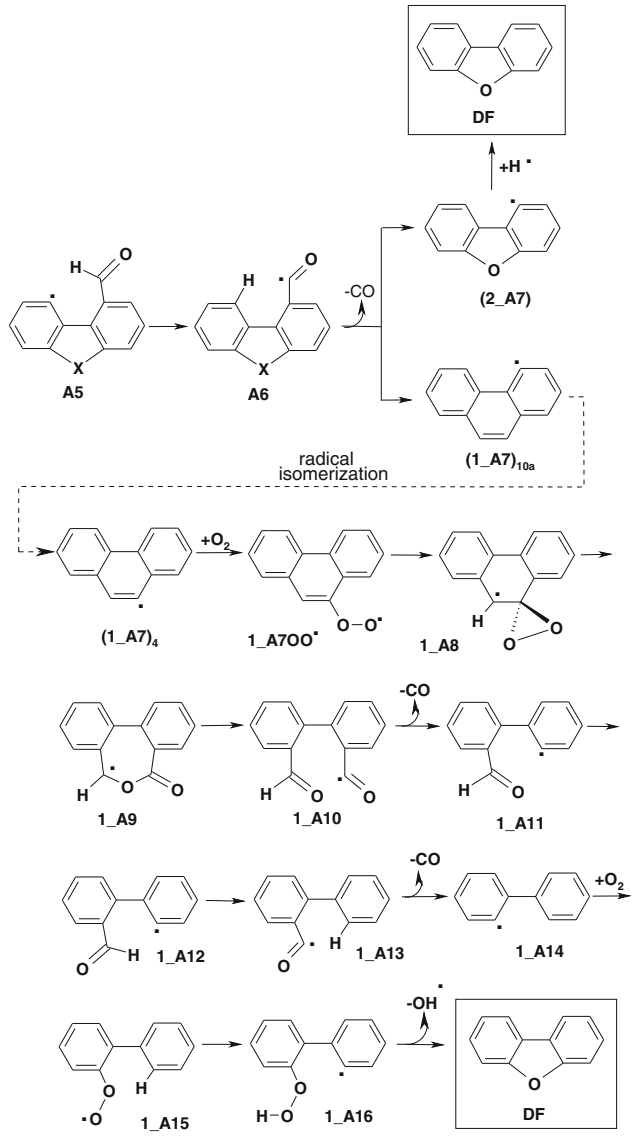

Scheme 7 Path from (**A5**) to DF

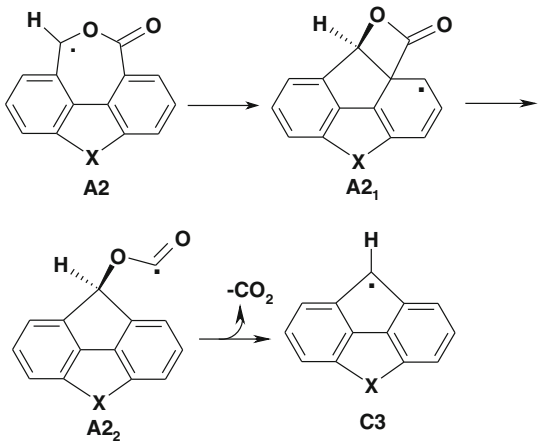

Scheme 8 Collateral path to A

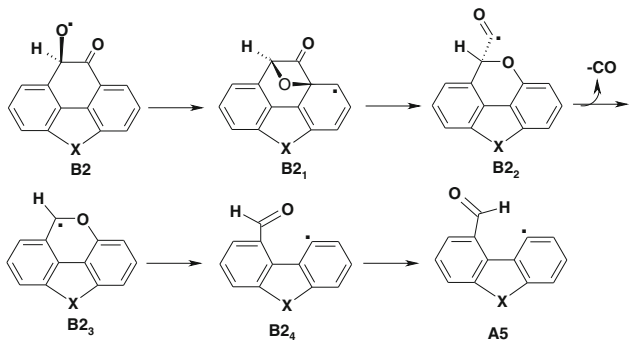

Scheme 9 Collateral path to B

producing the bicyclic structure (**B1**). The reaction involves the overcoming of a significant energetic barrier. Then, the O–O bond is cleaved: The (**B2**) intermediates are significantly more stable than (**B1**), due to the release of the steric hindrance imposed by the 4-membered ring. Successively, the C_9–C_{10} bond is cleaved, providing the dicarbonyl intermediates (**B3**) that, losing one CO molecule, provide van der Waals adducts between (**A5**) and the leaving CO molecule. As in path A, the intermediates and TSs between (**B2**) and (**A5**) of compound (**1**) are at higher energies than that of compound (**2**) due to their non-planar geometries.

An alternative route to (**A5**) starts from (**B2**), passes through the (**B2$_1$**)-(**B2$_4$**) intermediates and the loss of one CO molecule (Scheme 9, Table 4). The most significant barriers along this route involve (**B2$_1$**) and (**B2$_4$**) formation. The extent of these two barriers is due to the formation of the highly tensioned bicyclic structure (**B2$_1$**) and to the breaking of the C–O bond in the highly stable pyranyl-like structure (**B2$_3$**).

Path C. Path C involves O–O cleavage in (**Ar–OO$^{\cdot}$**) and the formation of the aryloxy radical (**C1**) and the ground-state oxygen atom, O(^{3}P) (Scheme 6, Table 3, Fig. 3). In the next step, a new bond between C_9 and C_{10a} is formed while the C_{10}–C_{10a} bond is broken in a concerted mechanism, overcoming the highest barrier along this path. Successively, a CO molecule is released, forming a van der Waals adduct with (**C3**). Evolution of (**C3**) involves reaction with another oxygen molecule, yielding the (**C4**) peroxy radical. Breaking the O–O bond yields the (**C5**) aryloxy radical and a ground-state oxygen atom, O(^{3}P). For this high endothermic step, no discrete TSs were observed. Finally, (**A5**) is obtained by opening the pentatomic ring. Contrary to paths A and B, here the path of compound (**2**) is at higher energy than that of compound (**1**), due to the presence of two condensed 5-membered rings.

As mentioned above, (**C3**) can also be obtained from (**A2**) through the path collateral to path A.

4.3 From (A5) to DF

At this point, the three paths, A, B, and C, converge to the common (**A5**) intermediate that continues in evolution towards the DF final product (Scheme 7, Table 5, Fig. 4). After a hydrogen transfer from the aldehydic moiety and CO expulsion, a van der Waals adduct between (**A7**) and CO is obtained. In the case of (**1_A5**), the step involves a variational transition state, with a lower energy, by 0.9 kcal mol^{-1}, than the reagent.

The (**2_A7**) intermediate can react with a hydrogen donor species (HX), providing the final DF product. Instead, the (**1_A7**) phenanthrenic radical requires further oxidative decomposition steps. Indeed, only the attack of a new O_2 molecule at the C_3 or C_4 positions can provide the DF final product; thus, only this path was considered. The starting step of this process must involve radical isomerization between (**1_A7**)$_{10a}$ and (**1_A7**)$_4$; such isomerization involves hydrogen migration that can occur via consecutive intra-molecular paths or via inter-molecular paths assisted by a HX species. Whatever the isomerization process, only the steps subsequent to (**1_A7**)$_4$ formation are analysed in the following.

The (**1_A7**)$_4$ undergoes the attack of O_2, forming the (**1_A7OO$^{\cdot}$**) peroxy radical that can follow three pathways analogous to those previously discussed for the phenyl and the (**Ar–OO$^{\cdot}$**) peroxy radicals. Those results show that path A involves the overcoming of lower energetic barriers with respect to paths B and C (see Discussion). For this reason, only the A-type path was investigated to characterize the route from (**1_A7OO$^{\cdot}$**) to DF.

The steps from (**1-A7OO$^{\cdot}$**) to the (**1_A14**) biphenyl radical have already been described for the case of Pyrene/BDF, and are not further discussed here. From the (**1_A14**) intermediate, the oxidation process to DF continues with the formation of the (**1_A15**) peroxy radical, by reaction with another oxygen molecule, and of the (**1_A16**) hydroperoxy radical, by transfer of a hydrogen atom. After conformational rearrangement of the C–C–O–O torsion, the closure of the furanic ring and the simultaneous expulsion of an OH radical leads to the final Dibenzofuran product.

5 Discussion

The oxidative pathway of compounds (**1**) and (**2**) to DF initially requires the formation of a radical species (Ar$^{\cdot}$), through the loss of a hydrogen atom. This occurs through reaction with molecular oxygen or radical species (X$^{\cdot}$) present in the environment and involves very different activation energies. In the case of the benzene reaction with molecular oxygen, a barrier of about 61 kcal mol^{-1} was

Table 3 PBE1PBE/6-311G** relative energies (ΔE, kcal mol^{-1}) calculated with respect to the peroxy radicals (**1-OO**$^{\cdot}$) or (**2-OO**$^{\cdot}$) for transition states and intermediates involved along paths A, B, and C

	Pyrene				BDF		
	ΔE^{a}	E_{att}	E_{react}		ΔE^{a}	E_{att}	E_{react}
1-OO$^{\cdot}$	0			**2-OO**$^{\cdot}$	0		
Path A							
(1OO-A1)$_{TS}$	22.2	22.2		**(2OO-A1)**$_{TS}$	22.8	22.8	
1_A1	11.4		11.4	**2_A1**	10.9		10.9
1_(A1-A2)$_{TS}$	27.9	16.5		**2_(A1-A2)**$_{TS}$	27.1	16.2	
1_A2	−44.6		−56.1	**2_A2**	−68.6		−79.6
1_(A2-A3)$_{TS}$	−19.5	25.1		**2_(A2-A3)**$_{TS}$	−49.1	19.5	
1_A3	−20.6		24.1	**2_A3**	−50.0		18.7
1_(A3A4)$_{TS}$	4.55	25.1		**2_(A3-A4)**$_{TS}$	−38.5	11.5	
1_W(A4-CO)	−0.22		20.4	**2_A4**	−47.8		2.2
1_A4	1.1		1.3	**2_(A4-A5)**$_{TS}$	−19.1	28.7	
1_(A4-A5)$_{TS}$	5.00	3.9		**2_W(A5-CO)**	−21.8		25.9
1_A5	−2.0		−3.0	**2_A5**	−21.2		0.6
Path B							
(1OO-B1)$_{TS}$	40.5	40.5		**(2OO-B1)**$_{TS}$	38.3	38.3	
1_B1	33.8		33.8	**2_B1**	29.8		29.8
1_(B1-B2)$_{TS}$	34.0	0.2		**2_(B1-B2)**$_{TS}$	30.3	0.4	
1_B2	−33.3		−67.1	**2_B2**	−36.7		−66.6
1_(B2-B3)$_{TS}$	−17.6	15.8		**2_(B2-B3)**$_{TS}$	−36.1	0.7	
1_B3	−18.6		14.7	**2_B3**	−47.8		−11.0
1_(B3-A5)$_{TS}$	3.0	21.7		**2_(B3-A5)**$_{TS}$	−19.1	28.7	
1_W(A5-CO)	−3.2		15.4	**2_W(A5-CO)**	−21.8		26.0
1_A5	−2.0		1.3	**2_A5**	−21.2		0.5
Path C							
(1OO-C1)$_{TS}$	31.4	31.4		**(2OO-C1)**$_{TS}$	31.8	31.8	
1-W(C1-O)	28.5		28.5	**2_W(C1-O)**	28.2		28.2
1_C1	30.9		2.4	**2_C1**	30.9		2.7
1_(C1-C2)$_{TS}$	91.3	60.4		**2_(C1-C2)**$_{TS}$	118.3	87.4	
1_C2	65.2		34.4	**2_C2**	97.3		66.4
1_(C2-C3)$_{TS}$	72.4	7.2		**2_(C2-C3)**$_{TS}$	104.1	6.8	
1_W(C3-CO)	60.1		−5.2	**2_W(C3-CO)**	93.0		−4.3
1_C3	60.5		0.4	**2_C3**	93.4		0.4
1_W(C3-O$_2$)	59.8		−0.7	**2_W(C3-O$_2$)**	92.7		−0.7
1_(C3-C4)$_{TS}$	64.9	5.1		**2_(C3-C4)**$_{TS}$	98.2	5.5	
1_C4	51.2		−8.6	**2_C4**	83.0		−9.7
1_C5	108.7		57.5	**2_C5**	139.4		56.4
1_(C5-A5)$_{TS}$	125.1	16.4		**2_(C5-A5)**$_{TS}$	145.0	5.6	
1_A5	117.4		8.7	**2_A5**	98.1		−41.3

Barriers (E_{att}, kcal mol^{-1}) and reaction energies ($E_{react} = E_{products} - E_{reagents}$, kcal mol^{-1}) for each step, are also reported. Transition states are labelled with TS subscript; van der Waals adducts includes a W in the name

[a] As an example: $\Delta E_{(1\_A5)} = [E_{(1\_A5)} + E_{(CO)}] - E_{(1\text{-}OO)}$ in path A and B; $\Delta E_{(1\_A5)} = [E_{(1\_A5)} + E_{(CO)} + 2\ E_{(O)}] - [E_{(1\text{-}OO)} + E_{(O2)}]$ in path C

found [13]. Hydrogen abstraction reactions in acenaphthylene, phenanthrene, naphthalene and biphenyl by H or CH_3 radicals involve activation energies in the range 7–10 kcal mol^{-1} [28]. Moreover, it is well known that copper and iron, as the metal itself or their oxides and salts, catalyse gas-carbon reactions, acting as a dissociation centre for O_2 chemisorption [3]. To overcome the problem of choosing a specific route to (**Ar**$^{\cdot}$) formation, we assumed

Table 4 PBE1PBE/6-311G** relative energies (ΔE, kcal mol^{-1}) calculated with respect to the peroxy radicals (**1-OO**$^{\cdot}$) or (**2-OO**$^{\cdot}$) for transition states and intermediates involved along collateral paths to A and B (see text for description)

Barriers (E_{att}, kcal mol^{-1}) and reaction energies ($E_{react} = E_{products} - E_{reagents}$, kcal mol^{-1}) for each step, are also reported. Transition states are labelled with TS subscript; van der Waals adducts includes a W in the name

	Pyrene				BDF		
	ΔE	E_{att}	E_{react}		ΔE	E_{att}	E_{react}
Collateral path to A							
1_A2	−44.6			**2_A2**	−68.6		
1_(A2-A2$_1$)$_{TS}$	−17.8	26.8		**2_(A2-A2$_1$)$_{TS}$**	−9.9	58.8	
1_A2$_1$	−32.1		12.5	**2_A2$_1$**	−12.4		56.2
1_(A2$_1$-A2$_2$)$_{TS}$	−20.0	12.2		**2_(A2$_1$-A2$_2$)$_{TS}$**	6.0	18.5	
1_A2$_2$	−29.9		2.3	**2_A2$_2$**	2.1		14.6
1_(A2$_2$-C3)$_{TS}$	−12.5	17.4		**2_(A2$_2$-C3)$_{TS}$**	21.6	19.5	
1_W(C3-CO$_2$)	−71.5		−41.6	**2_W(C3-CO$_2$)**	−38.6		−40.8
1_C3	−70.3		1.2	**2_C3**	−37.4		1.3
Collateral path to B							
1_B2	−33.3			**2_B2**	−36.7		
1_(B2-B2$_1$)$_{TS}$	−9.9	23.4		**2_(B2-B2$_1$)$_{TS}$**	−4.0	32.7	
1_B2$_1$	−18.4		14.9	**2_B2$_1$**	−7.2		29.5
1_(B2$_1$-B2$_2$)$_{TS}$	−12.4	6.0		**2_(B2$_1$-B2$_2$)$_{TS}$**	−2.1	5.1	
1_B2$_2$	−33.0		−14.6	**2_B2$_2$**	−28.8		−21.5
1_(B2$_2$-B2$_3$)$_{TS}$	−29.8	3.2		**2_(B2$_2$-B2$_3$)$_{TS}$**	−24.6	4.2	
1_W(B2$_3$-CO)	−41.5		−8.5	**2_W(B2$_3$-CO)**	−35.3		−6.5
1_B2$_3$	−41.4		0.1	**2_B2$_3$**	−34.6		0.6
1_(B2$_3$- B2$_4$)$_{TS}$	6.3	47.7		**2_(B2$_3$-B2$_4$)$_{TS}$**	0.2	34.9	
1_B2$_4$	1.1		42.5	**2_B2$_4$**	−21.0		13.6
1_(B2$_4$-A5)$_{TS}$	5.00	3.9		**2_(B2$_4$-A5)$_{TS}$**	−12.4	8.6	
1_A5	−2.0		−3.0	**2_A5**	−21.2		−0.2

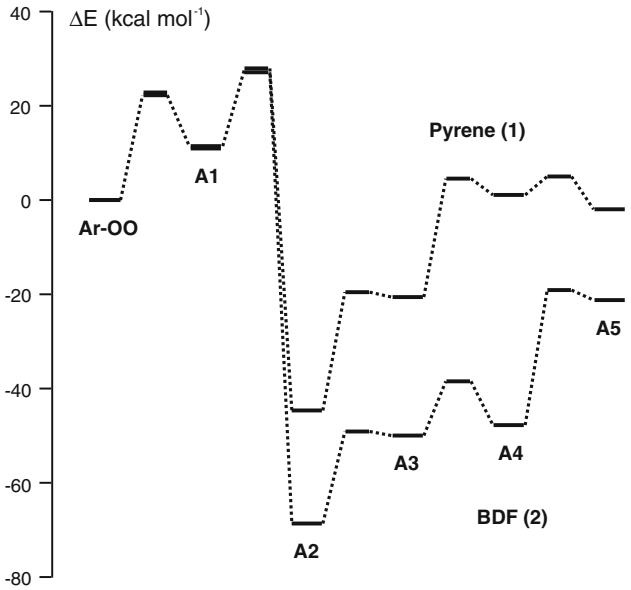

Fig. 1 Relative energies (ΔE, kcal mol^{-1}), calculated with respect to (**Ar–OO**$^{\cdot}$), along path A for Pyrene (**1**) and Benzodibenzofuran (**2**)

the (**Ar**$^{\cdot}$) species to be already formed, regardless of the reactions involved.

The attack of molecular oxygen to non-equivalent positions in (**Ar**$^{\cdot}$) provides different (**Ar–OO**$^{\cdot}$) peroxy radicals that undergo different oxidative paths, as in the case of the phenyl radical [17]. However, only some of these paths lead to the formation of DF, and it is these that were investigated.

Once formed, the (**Ar–OO**$^{\cdot}$) peroxy radical can follow three possible paths (A, B and C) to the (**A5**) common intermediate. It is noteworthy that the first step along the three paths presents similar activation energies to the corresponding steps in vinyl, phenyl and Dibenzofuranyl peroxy radical reactions. This finding further supports analogies already observed for olefinic and aromatic systems [14].

Compounds (**1**) and (**2**) present similar energetic profiles in the three paths, but the paths show different features.

Along path A, the highest energetic barrier corresponds to the CO release step, with a barrier of 25.1 and 28.7 kcal mol^{-1} for compounds (**1**) and (**2**), respectively. From (**A2**), the path of compound (**2**) is always at lower energy than that of compound (**1**), which presents non-planar intermediates due to the steric hindrance between the orto substituents.

In path B, the highest barrier is found in the first step involving intramolecular cyclization to (**B1**), with barriers of 40.5 and 38.3 kcal mol^{-1} for compounds (**1**) and (**2**), respectively. Also in path B, compound (**2**) intermediates are lower in energy than those of compound (**1**), because of the non-planarity of Pyrene intermediates.

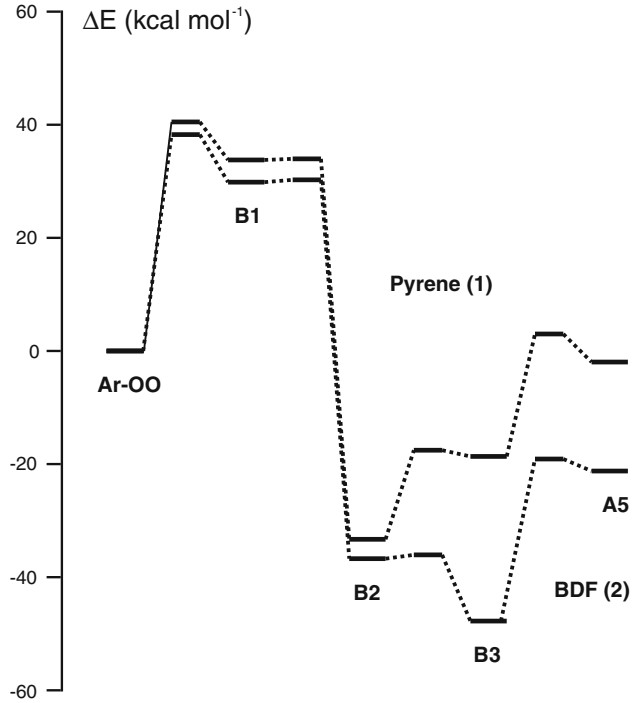

Fig. 2 Relative energies (ΔE, kcal mol^{-1}), calculated with respect to (**Ar–OO**$^{\cdot}$), along path B for Pyrene (**1**) and Benzodibenzofuran (**2**)

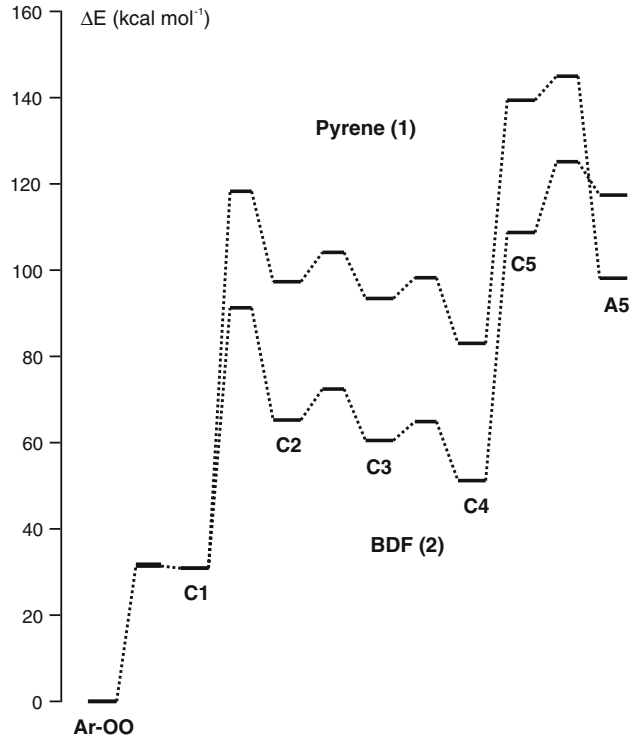

Fig. 3 Relative energies (ΔE, kcal mol^{-1}), calculated with respect to (**Ar–OO**$^{\cdot}$), along path C for Pyrene (**1**) and Benzoidbenzofuran (**2**)

Along path C, both compounds encounter the highest barrier in the formation of the 5-membered ring, (**C1**) to (**C2**) step, with barriers of 60.4 and 87.4 kcal mol^{-1}, respectively. Here, the Pyrene intermediates are planar while those of (**2**) are bent due to the presence of two condensed penta-atomic rings. Thus in this case compound (**1**), intermediates lie at a lower energy than those of compound (**2**).

Two possible collateral paths were also identified. The first starts from (**A2**) and leads to the (**C3**) intermediate, losing a CO_2 molecule. This route to (**C3**) is competitive with path C as it involves the overcoming of lower barriers, 26.8 and 58.8 kcal mol^{-1} for compounds (**1**) and (**2**), respectively. The second collateral path starts from (**B2**) and leads to the formation of the (**A5**) intermediate. This route is not competitive with path B as it involves the overcoming of a significant barrier (47.7 and 34.9 kcal mol^{-1}, for compounds (**1**) and (**2**), respectively) when the C–O bond in the (**B2$_3$**) pyranyl-like structure is broken.

As a general remark, the different steric constraints in compounds (**1**) and (**2**) imposed by the presence of a benzenic or a furanic ring condensed to the phenanthrenic system affects the planarity of the intermediates along the three paths. This molecular characteristic plays a role in determining the relative stability of the intermediates but affects the energetic barriers to a lesser extent, at least in the case of path A.

Comparison between the different paths of compounds (**1**) and (**2**) to (**A5**) shows that path A is always the kinetically favoured one, and the highest barrier is encountered when the CO molecule is released. In the case of compound (**1**), the highest barrier (26.8 kcal mol^{-1}) in the collateral channel involving CO_2 release and (**C3**) formation is comparable with that involving CO release in path A (25.1 kcal mol^{-1}). However, during the reaction steps from (**C3**) to (**A5**), a significant barrier of 57.5 kcal mol^{-1} has to be overcome.

Evolution of the (**A5**) intermediate involves the release of another CO molecule, overcoming barriers of 26.5 and 30.1 kcal mol^{-1} for the respective compounds (**1**) and (**2**), with the formation of the Phenanthrene (**1_A7**) and Dibenzofuran (**2_A7**) radicals. While compound (**2**) completes its oxidative path to DF, the (**1_A7**) radical must undergo further steps towards the final DF product. The first step involves a radical isomerization between C_{10a} and C_4. As previously noted for (**Ar**$^{\cdot}$) formation, the presence of a hydrogen donor HX species in the reaction environment can assist the isomerization process, lowering the high barriers (about 60 kcal mol^{-1}) expected for an intramolecular mechanism. Once the (**1_A7**)$_4$ radical has been formed, four high energetic barriers (23–29 kcal mol^{-1}) are encountered towards DF formation; two of these barriers involve the loss of a CO molecule.

Our results can be compared with temperature-programmed desorption (TPD) spectra from disperse

Table 5 PBE1PBE/6-311G** relative energies (ΔE, kcal mol^{-1}) calculated with respect to the peroxy radicals (**1-OO**$^{\cdot}$) or (**2-OO**$^{\cdot}$) for transition states and intermediates from (**A5**) to DF

	Pyrene				BDF		
	ΔE	E_{att}	E_{react}		ΔE	E_{att}	E_{react}
1-A5	−2.0			**2_A5**	−21.2		
1_(A5-A6)$_{TS}$	−2.9	−0.9		**2_(A5-A6) $_{TS}$**	−8.3	13.0	
1-A6	−21.6		−19.7	**2_A6**	−43.9		−22.7
1_(A6-A7)$_{TS}$	4.8	26.5		**2_(A6-A7) $_{TS}$**	−13.9	30.1	
1_W(A7-CO)	2.0		23.7	**2_W(A7-CO)**	−14.4		29.5
(1_A7)$_{10a}$	2.8		0.8	**2_A7**	−13.7		0.8
(1_A7)$_4$	4.6		−0.1				
1_A7OO$^{\cdot}$	−39.5						
1_(A7OO-A8)$_{TS}$	−16.9	22.6					
1_A8	−27.1		12.4				
1_(A8-A9)$_{TS}$	−10.8	16.3					
1_A9	−86.4		−59.2				
1_(A9-A10)$_{TS}$	−63.2	23.1					
1_A10	−65.9		20.4				
1_(A10-A11)$_{TS}$	−39.7	26.3					
1_W(A11-CO)	−41.1		24.8				
1_A11	−39.8		1.3				
1-(A11-A12) $_{TS}$	−35.5	4.4					
1_A12	−42.8		−3.0				
1_(A12-A13)$_{TS}$	−42.1	0.7					
1-A13	−64.9		−22.1				
1_(A13-A14) $_{TS}$	−36.2	28.7					
1_W(A14-CO)	−37.8		27.0				
1_A14	−37.1		0.8				
1_W(A14-O$_2$)	−38.0		−1.0				
1_(A14-A15) $_{TS}$	−37.9	0.1					
1_A15	−75.6		−37.6				
1_(A15-A16) $_{TS}$	−50.3	25.3					
1_A16	−49.1		26.5				
1_(A16-A16′) $_{TS}$	−48.5	0.6					
1_A16′	−49.6		−0.4				
1_(A16′-DF) $_{TS}$	−42.6	6.5					
1_W(DF-OH)	−118.1		−69.0				
DF	−113.5		4.6	**DF**	−121.9		−108.2

Barriers (E_{att}, kcal mol^{-1}) and reaction energies ($E_{react} = E_{product} - E_{reagents}$, kcal mol^{-1}) for each step, are also reported. Transition states are labelled with TS subscript; van der Waals adducts includes a W in the name

polycrystalline graphite oxidized with CO [29]. These spectra show two main broad CO evolution features in the 973–1,253 K and 400–700 K range. Activation desorption energies (64–83 kcal mol^{-1}) derived from high-temperature measurements have been associated with the desorption of a CO group belonging to 6-membered ring systems (usually referred to in the literature as semiquinone). In the low-temperature range, activation desorption energies (25–44 kcal mol^{-1}) have been associated with CO desorption from ketene structures. Indeed, in our calculations, along path A and along the route from (**A5**) to DF, the highest energetic barriers are always encountered in the steps where a CO molecule is released from ketene-like structures, the values spanning 25–30 kcal mol^{-1}. Moreover, along path C, the rate determining step in CO desorption is the rearrangement of the (**C1**) semiquinone structure, involving a barrier of 60.4 and 87.4 kcal mol^{-1} in compounds (**1**) and (**2**), respectively. Thus, our results compare well with the reported TPD energies and structural features proposed by Marchon et al. [29].

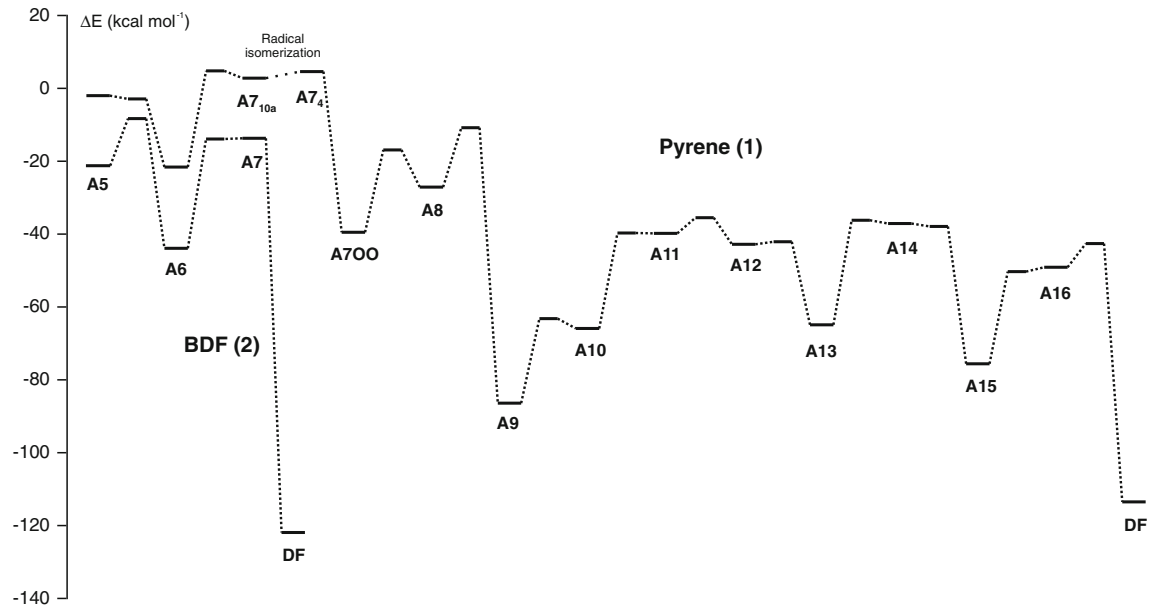

Fig. 4 Evolution from (**A5**) to DF: relative energies (ΔE, kcal mol^{-1}) calculated with respect to (**Ar–OO**$^{\cdot}$), for Pyrene (**1**) and Benzodibenzofuran (**2**)

Our results also agree with the experimental evidence obtained for the oxidation of Pyrene [9] that shows the formation, among other trace compounds, of DF, phenanthrene and biphenyl. Indeed, along our calculated path, we observed the formation of both (**1_A7**) phenanthrene and (**1_A14**) biphenyl radicals.

6 Conclusion

The present work is a first attempt to shed light on the mechanism of PCDD/F formation by de novo synthesis, a trace reaction that occurs in the "cold zones" of flue gas control devices of MSW incinerators. The aim of studying such formation mechanisms is to find a way to prevent and/or minimize PCDD/F formation.

Here we propose a model for the de novo synthesis of Dibenzofuran from Pyrene and Benzodibenzofuran, chosen as model compounds of carbonaceous material present in fly-ash. Our calculations have led to the identification of a kinetically preferred pathway, though the temperature dependence of energetic barriers could increase the relevance of other higher energetic paths.

Along the preferred pathway, different steric constraints in compounds (**1**) and (**2**) play a role in determining the relative stability of the intermediates; however, such constraints have less influence on the energetic barriers. Thus, we believe that compounds (**1**) and (**2**) should present similar kinetic behaviour as the energetic barriers to be overcome are similar.

Future work will investigate the reciprocal influence of chlorination and oxidation reactions in polychlorinated Dibenzofuran formation.

Acknowledgments We gratefully acknowledge financial support from the University of Milano-Bicocca (FAR2010). We wish to thank Prof. V. Barone, Scuola Normale di Pisa, Italy, for his constant encouragement and stimulating discussions.

References

1. Grandesso E, Ryan S, Gullett B, Touati A, Collina E, Lasagni M, Pitea D (2008) Kinetic modeling of polychlorinated Dibenzo-*p*-Dioxin and dibenzofuran formation based on carbon degradation reactions. Environ Sci Technol 42:7218–7224
2. Altarawneh M, Dlugogorski BZ, Kennedy EM, Mackie JC (2009) Mechanisms for formation, chlorination, dechlorination and destruction of polychlorinated Dibenzo-*p*-Dioxins and dibenzofurans (PCDD/Fs). Prog Energy Combust Sci 35:245–274
3. Huang H, Buekens A (1996) De novo synthesis of polychlorinated Dibenzo-*p*-Dioxins and dibenzofurans. Proposal of a mechanistic scheme. Sci Total Environ 193:121–141
4. Stanmore BR (2004) The formation of dioxins in combustion systems. Combust Flame 136:398–427
5. Pitea D, Bortolami M, Collina E, Cortili G, Franzoni F, Lasagni M, Piccinelli E (2008) Prevention of PCDD/F formation and minimization of their emission at the stack of a secondary aluminum casting plant. Environ Sci Technol 42:7476–7481
6. Iino F, Imagawa T, Takeuchi M, Sadakata M (1999) De novo synthesis mechanism of polychlorinated dibenzofurans from polycyclic aromatic hydrocarbons and the characteristic isomers of polychlorinated naphthalenes. Environ Sci Technol 33:1038–1043

7. Weber R, Iino F, Imagawa T, Takeuchi M, Sakurai T, Sadakata M (2001) Formation of PCDF, PCDD, PCB, and PCN in de novo synthesis from PAH: mechanistic aspects and correlation to fluidized bed incinerators. Chemosphere 44:1429–1438
8. DeCoster J, Ergut A, Levendis YA, Richter H, Howard JB, Carlson JB (2007) PAH emissions from high-temperature oxidation of vaporized anthracene. Proc Combust Inst 31:491–499
9. Fullana A, Sidhu SS (2005) Fate of PAHs in the post-combustion zone: partial oxidation of PAHs to dibenzofuran over CuO. J Anal Appl Pyrolysis 74:479–485
10. Marquaire P, Worner R, Rambaud P, Baronnet F (1999) Organohalogen Compd 40:419–422
11. Marquaire PM, Bounaceur R, Baronnet F (2003) Detailed mechanism of dibenzofuran oxidation. Organohalogen Compd 63:377–380
12. Marquaire PM, Wörner R, Baronnet F (2002) Dioxins abatement by total oxidation. IT3'02 conference, May 13–17, New Orleans, Louisiana
13. Altarawneh M, Dlugogorski BZ, Kennedy EM, Mackie JC (2006) Quantum chemical study of low temperature oxidation mechanism of dibenzofuran. J Phys Chem A 110:13560–13567
14. Sebbar N, Bockhorn H, Bozzelli JW (2008) Thermochemical similarities among three reaction systems: Vinyl + O_2 − Phenyl + O_2 − Dibenzofuranyl + O_2. Combust Sci Tech 180:959–974
15. Altarawneh M, Dlugogorski BZ, Kennedy EM, Mackie JC (2007) Theoretical study of reaction pathways of dibenzofuran and Dibenzo-*p*-Dioxin under reducing conditions. J Phys Chem A 111:7133–7140
16. Mebel AM, Diau EWG, Lin MC, Morokuma K (1996) Ab initio and RRKM calculations for multichannel rate constants of the $C_2H_3 + O_2$ reaction. J Am Chem Soc 118:9759–9771
17. Tokmakov IV, Kim-Sue G, Kislov VV, Mebel AM, Lin MC (2005) The reaction of phenyl radical with molecular oxygen: a G2 M study of the potential energy surface. J Phys Chem A 109:6114–6127
18. Sebbar N, Bockhorn H, Bozzelli J (2008) Thermodynamic properties of the species resulting from the phenyl radical with O_2 reaction system. Int J Chem Kinet 40:583–604
19. Sebbar N, Bockhorn H, Bozzelli JW (2005) Thermochemical properties, rotation barriers, and group additivity for unsaturated oxygenated hydrocarbons and radicals resulting from reaction of vinyl and phenyl radical systems with O_2. J Phys Chem A 109:2233–2253
20. Sebbar N, Bockhorn H, Bozzelli JW (2004) Thermochemical properties, rotation barriers, bond energies, and group additivity for vinyl, phenyl, ethynyl, and allyl peroxides. J Phys Chem A 108:8353–8366
21. Ghigo G, Maranzana A, Tonachini G, Zicovich-Wilson CM, Causà M (2004) Modeling soot and its functionalization under atmospheric or combustion conditions by density functional theory within molecular (Polycyclic-Aromatic-Hydrocarbon-like) and periodic methodologies. J Phys Chem B 108:3215–3223
22. Perry ST, Hambly EM, Fletcher TH, Solum MS, Pugmire RJ (2000) Solid-state 13C NMR characterization of matched tars and chars from rapid coal devolatilization. Proc Combust Inst 28:2313–2319
23. Homann KH (1998) Fullerenes and soot formation: new pathways to large particles in flames. Angew Chem Int Ed 37:2434–2451
24. Frisch MJ, Trucks GW, Schlegel HB, Scuseria GE, Robb MA, Cheeseman JR, Scalmani G, Barone V, Mennucci B, Petersson GA, Nakatsuji H, Caricato M, Li X, Hratchian HP, Izmaylov AF, Bloino J, Zheng G, Sonnenberg JL, Hada M, Ehara M, Toyota K, Fukuda R, Hasegawa J, Ishida M, Nakajima T, Honda Y, Kitao O, Nakai H, Vreven T, Montgomery JrJA, Peralta JE, Ogliaro F, Bearpark M, Heyd JJ, Brothers E, Kudin KN, Staroverov VN, Kobayashi R, Normand J, Raghavachari K, Rendell A, Burant JC, Iyengar SS, Tomasi J, Cossi M, Rega N, Millam NJ, Klene M, Knox JE, Cross JB, Bakken V, Adamo C, Jaramillo J, Gomperts R, Stratmann RE, Yazyev O, Austin AJ, Cammi R, Pomelli C, Ochterski JW, Martin RL, Morokuma K, Zakrzewski VG, Voth GA, Salvador P, Dannenberg JJ, Dapprich S, Daniels AD, Farkas Ö, Foresman JB, Ortiz JV, Cioslowski J, Fox DJ (2009) Gaussian 09, Revision A.02. Gaussian Inc. Wallingford CT
25. Adamo C, Barone V (2002) Physically motivated density functionals with improved accuracy: the modified Perdew-Burke-Ernzerhof model. J Chem Phys 116:5933–5940
26. Menon AS, Radom L (2008) Consequences of spin contamination in unrestricted calculations on open-shell species: effect of Hartree–Fock and Møller–Plesset contributions in hybrid and double-hybrid density functional theory approaches. J Phys Chem A 112:13225–13230
27. Mebel AM, Morokuma K, Lin MC (1995) Modification of the Gaussian-2 theoretical model: the use of coupled-cluster energies, density-functional geometries, and frequencies. J Chem Phys 103:7414–7421
28. Carissan Y, Klopper W (2010) Hydrogen abstraction from biphenyl, acenaphthylene, naphthalene and phenanthrene by atomic hydrogen and methyl radical: DFT and G3(MP2)-RAD data. J Mol Struct THEOCHEM 940:115–118
29. Marchon B, Tysoe WT, Carrazza J, Heinemann H, Somorjai GA (1988) Reactive and kinetic properties of carbon monoxide and carbon dioxide on a graphite surface. J Phys Chem 92:5744–5749